

Observable acceleration of jets by a Kerr black hole

J. Gariel^{1,*}, N. O. Santos^{1,3,†} and Anzhong Wang^{4,5,6‡}

¹*Sorbonne Universités, UPMC Université Paris 06, LERMA,
UMRS8112 du CNRS, Observatoire de Paris-Meudon 5,
Place Jules Janssen, F-92195 Meudon Cedex, France*

³*School of Mathematical Sciences, Queen Mary, University of London, London E1 4NS, UK*

⁴*GCAP-CASPER, Department of Physics, Baylor University, Waco, Texas 76798-7316, USA*

⁵*Institute for Advanced Physics & Mathematics,*

Zhejiang University of Technology, Hangzhou 310032, China

⁶*Departamento de Física Teórica, Instituto de Física, UERJ, 20550-900, Rio de Janeiro, Brazil*

In the framework of a model based on the gravitational field of the Kerr black hole, we turn to investigate the kinematic behavior of extragalactic jets. We analytically calculate the observable velocities and accelerations along any geodesic. Then, by numerical calculations, we apply our results to a geodesic, typical of the M87 jet, and probe our results by confrontation to recent observations. A transition from non-relativistic to ultrarelativistic speeds at subparsec scale is highlighted. This transition comes sooner and more abruptly than in models based on magnetic paradigm, which indicates that we need a weaker magnetic field to explain observed synchrotron radiation. We attribute the ejection phenomenon to the repulsive effect of the gravitomagnetic Kerr field.

I. INTRODUCTION

The extragalactic jets are important astrophysical phenomena generated by central engines supposed to be black holes (BH). Inspired by the theory of jets ejected from less exotic sources, as usual stars and neutron stars, the first models were based on the electromagnetic field, with magnetic field lines anchored in the BH horizon [1], or in the accretion disk [2], including magnetohydrodynamics [3]. Until today, these standard models remain the main paradigm used as basis for confrontations with the observations. The raised questions for probing the models concern, inter alia, the shape, the length and permanence, the profile, the power, the radiation, the composition, the acceleration, and the birth of the jet. Here, we shall focus on the acceleration at the launching.

The initial acceleration of the jet is currently assumed to be of magnetic origin, and all the observations are confronted to models inside this framework [12, 14]. We propose a model mainly based on the gravitational field. In General Relativity (GR) the only axisymmetric stationary metric with a good asymptotic behavior is the Kerr BH. We first analyze the admissible collimation [6], the high energies [11], the profile of the M87 jet [7], and the Penrose effect [8]. Then, we turn to kinematical studies by considering the proper acceleration along the axis of symmetry, showing the clear existence of a repulsive effect [9]. Here we deepen this study by calculating the observable velocities and accelerations. After recalling the basic equations (section II) and previous results (section III), we analytically calculate the proper acceleration along the radial ρ -component (section IV) and the

temporal variation (Section V), the observable velocity and acceleration (Section VI). Then, by numerical calculations, we apply our results to a geodesic, typical of the M87 jet as studied in [7], and compare our results with the observations [12, 14] (Section VII). In Section VIII, we summarize our main results with a brief discussion.

II. RECALLING THE KERR GEODESICS IN WEYL COORDINATES

The Kerr metric given in the usual Boyer-Lindquist spherical coordinates \bar{r} , θ and ϕ reads

$$ds^2 = - \left(\frac{\bar{r}^2 - 2M\bar{r} + a^2}{\bar{r}^2 + a^2 \cos^2 \theta} \right) (d\bar{t} - a \sin^2 \theta d\phi)^2 + \frac{\sin^2 \theta}{\bar{r}^2 + a^2 \cos^2 \theta} [a d\bar{t} - (\bar{r}^2 + a^2) d\phi]^2 + (\bar{r}^2 + a^2 \cos^2 \theta) \left(\frac{d\bar{r}^2}{\bar{r}^2 - 2M\bar{r} + a^2} + d\theta^2 \right), \quad (1)$$

where M and $J \equiv Ma$ are, respectively, the mass and the angular momentum of the source, and we have taken units such that $c = G = 1$ where G is Newton's constant of gravitation. Rescaling the \bar{t} and \bar{r} coordinates as $t = \bar{t}/M$ ($s = \bar{r}/M$) and $r = \bar{r}/M$ the timelike geodesics equations are

$$\dot{r}^2 = (a_4 r^4 + a_3 r^3 + a_2 r^2 + a_1 r + a_0) \times \left[r^2 + \left(\frac{a}{M} \right)^2 \cos^2 \theta \right]^{-2}, \quad (2)$$

$$\dot{\theta}^2 = \frac{b_4 \cos^4 \theta + b_2 \cos^2 \theta + b_0}{1 - \cos^2 \theta} \times \left[r^2 + \left(\frac{a}{M} \right)^2 \cos^2 \theta \right]^{-2}, \quad (3)$$

*Electronic address: jerome.gariel@obspm.fr

†Electronic address: n.o.santos@qmul.ac.uk

‡Electronic address: anzhong.wang@baylor.edu

with coefficients

$$a_0 = -\frac{a^2 Q}{M^4} = -\left(\frac{a}{M}\right)^2 b_0, \quad (4)$$

$$a_1 = \frac{2}{M^2} [(aE - L_z)^2 + Q], \quad (5)$$

$$a_2 = \frac{1}{M^2} [a^2(E^2 - 1) - L_z^2 - Q], \quad (6)$$

$$a_3 = 2, \quad (7)$$

$$a_4 = E^2 - 1, \quad (8)$$

and

$$b_0 = \frac{Q}{M^2}, \quad (9)$$

$$b_2 = \frac{1}{M^2} [a^2(E^2 - 1) - L_z^2 - Q] = a_2, \quad (10)$$

$$b_4 = -\left(\frac{a}{M}\right)^2 (E^2 - 1) = -\left(\frac{a}{M}\right)^2 a_4, \quad (11)$$

where a dot stands for differentiation with respect to the dimensionless proper time τ , and E , L_z and Q are integration constants of motion. Here Chandrasekhar's particle mass $\sqrt{\delta_1}$ [4] has been set to one, its value for time-like geodesics, and E and L_z have the usual significance of total energy and angular momentum about the z axis, both quantities given by units of $\sqrt{\delta_1}$, and Q is the Carter constant given by units of δ_1 . With this understanding, E is dimensionless, while L_z and Q have dimensions of M and M^2 , respectively. All the a_i and b_i are dimensionless. In this paper we consider only particles moving along unbound geodesics with $E \geq 1$ [4].

In order to understand better the physical meaning of the Kerr geodesics we use Weyl cylindrical coordinates ρ , z and ϕ which are more revealing and, in a way, a natural choice for axially symmetric systems [6, 8, 9]. The dimensionless Weyl cylindrical coordinates, in multiples

of geometrical units of mass M , are given by

$$\rho = [(r-1)^2 - A]^{1/2} \sin \theta, \quad z = (r-1) \cos \theta, \quad (12)$$

where

$$A = 1 - \left(\frac{a}{M}\right)^2. \quad (13)$$

From (12) we have the inverse transformation

$$r = \alpha + 1, \quad (14)$$

$$\sin \theta = \frac{\rho}{(\alpha^2 - A)^{1/2}}, \quad \cos \theta = \frac{z}{\alpha}, \quad (15)$$

with

$$\alpha = \frac{1}{2} \left\{ \left[\rho^2 + (z + \sqrt{A})^2 \right]^{1/2} + \left[\rho^2 + (z - \sqrt{A})^2 \right]^{1/2} \right\}. \quad (16)$$

Here we have assumed $A \geq 0$, and taken the root of the second degree equation obtained from (15) for the function $\alpha(\rho, z)$ that allows the extreme black hole limit $A = 0$. The other root in this limit is $\alpha = 0$.

Now, with (14) and (15) we can rewrite the geodesics (2) and (3) in terms of ρ , z and t coordinates, producing the following autonomous system of first order equations

$$\dot{\rho} = \frac{1}{U} \left[\frac{P \alpha^3 \rho}{\alpha^2 - A} + \frac{S(\alpha^2 - A)z}{\alpha \rho} \right], \quad (17)$$

$$M \dot{z} = \frac{1}{U} (Pz - S)\alpha, \quad (18)$$

$$\dot{t} = \frac{\alpha^2}{U \Delta} \left[\Sigma^2 E - 2 \frac{a}{M} (\alpha + 1) \frac{L_z}{M} \right], \quad (19)$$

where

$$P = [a_4(\alpha + 1)^4 + a_3(\alpha + 1)^3 + a_2(\alpha + 1)^2 + a_1(\alpha + 1) + a_0]^{1/2}, \quad (20)$$

$$S = -(b_4 z^4 + b_2 \alpha^2 z^2 + b_0 \alpha^4)^{1/2}, \quad (21)$$

$$U = (\alpha + 1)^2 \alpha^2 + \left(\frac{a}{M}\right)^2 z^2, \quad (22)$$

$$\Delta = (\alpha + 1)^2 - 2(\alpha + 1) + \left(\frac{a}{M}\right)^2 = \alpha^2 + \left(\frac{a}{M}\right)^2 - 1 = \alpha^2 - A, \quad (23)$$

$$\Sigma^2 = \left[(\alpha + 1)^2 + \left(\frac{a}{M}\right)^2 \right]^2 + \left(\frac{a}{M}\right)^2 \left[\left(\frac{z}{\alpha}\right)^2 - 1 \right] \Delta, \quad (24)$$

with the sign of S chosen to indicate outgoing particles [6].

Our aim is to study geodesics that can attain large distances while becoming parallels to the axis z , which corresponds to the condition $z \gg \rho$. For this limit, from

(21) we find

$$S \approx -[(b_0 + b_2 + b_4)z^4 + (2b_0 + b_2)\rho^2 z^2]^{1/2} + O(z^{-1}), \quad (25)$$

where

$$b_0 + b_2 + b_4 = -\left(\frac{L_z}{M}\right)^2 \leq 0, \quad (26)$$

$$2b_0 + b_2 = \frac{1}{M^2} [a^2(E^2 - 1) - L_z^2 + Q]. \quad (27)$$

Hence in this limit S is well defined and real for indefinitely small ρ/z only for $L_z = 0$. The geodesics obeying this restriction, imposed after similar reasoning, were studied in [5], but in Boyer-Lindquist or Kerr-Schild coordinates.

From now on we consider that a and L_z are also expressed in units of M and Q in units of M^2 , which is equivalent to put $M = 1$ in a/M , L_z/M and Q/M^2 .

III. PROPER ACCELERATION ALONG THE z AXIS

We would like now to calculate the proper acceleration \ddot{z} of a particle along the z axis. Taking the second proper time derivative of (18) produces (see [9])

$$U^2 \ddot{z} = U(\dot{P}z - \dot{S})\alpha + \left[UP - 2\left(\frac{a}{M}\right)^2 (Pz - S)z\right]\alpha \dot{z} + (Pz - S)[U - 2\alpha^2(\alpha + 1)(2\alpha + 1)]\dot{\alpha}. \quad (28)$$

From (7), (20) and (21) we have

$$U(\dot{P}z - \dot{S}) = \frac{1}{2} [4a_4(\alpha + 1)^3 + 3a_3(\alpha + 1)^2 + 2a_2(\alpha + 1) + a_1] \alpha^2 z - 2PS\alpha + (2b_4z^2 + b_2\alpha^2)\alpha z. \quad (29)$$

Substituting (18) and (29) into (28) we obtain

$$\begin{aligned} \frac{U^3}{\alpha^2} \ddot{z} = & \frac{U}{2} [4a_4(\alpha + 1)^3 + 3a_3(\alpha + 1)^2 + 2a_2(\alpha + 1) + a_1] \alpha z + U[(2b_4z^2 + b_2\alpha^2)z - 2PS] \\ & + 2(Pz - S)\left[UP - \left(\frac{a}{M}\right)^2 (Pz - S)z\right] - 2(Pz - S)P\alpha^2(\alpha + 1)(2\alpha + 1), \end{aligned} \quad (30)$$

or

$$\begin{aligned} \frac{U^3}{\alpha^2} \ddot{z} = & \frac{U}{2} [4a_4(\alpha + 1)^3 + 3a_3(\alpha + 1)^2 + 2a_2(\alpha + 1) + a_1] \alpha z + U(2b_4z^2 + b_2\alpha^2)z - 2P^2\alpha^3(\alpha + 1)z \\ & - 2\left(\frac{a}{M}\right)^2 S^2 z - 2PS\alpha^2(\alpha + 1). \end{aligned} \quad (31)$$

Substitution of (20), (21) and (22) into (30) gives

$$\begin{aligned} \frac{U^3}{\alpha^2} \ddot{z} = & -\frac{1}{2} [a_3(\alpha + 1)^3 + 2a_2(\alpha + 1)^2 + 3a_1(\alpha + 1) + 4a_0] \alpha^3(\alpha + 1)z + \frac{1}{2}\left(\frac{a}{M}\right)^2 [4a_4(\alpha + 1)^3 + 3a_3(\alpha + 1)^2 \\ & + 2a_2(\alpha + 1) + a_1] \alpha z^3 + (2b_4z^2 + b_2\alpha^2)\alpha^2(\alpha + 1)^2 z - \left(\frac{a}{M}\right)^2 (b_2z^2 + 2b_0\alpha^2)\alpha^2 z - 2PS\alpha^2(\alpha + 1). \end{aligned} \quad (32)$$

Now considering (4), (7), (10) and (11) and then substituting them into (32) we have

$$\begin{aligned} \frac{U^3}{\alpha^3} \ddot{z} = & -(\alpha + 1)^4 \alpha^2 z - \left[\left(a_2 + \frac{3}{2}a_1\right)(\alpha + 1)^2 + 2a_0\right] \alpha^2 z + \left(\frac{a}{M}\right)^2 \left[(2a_4 + 3)(\alpha + 1)^2 + a_2 + \frac{1}{2}a_1\right] z^3 \\ & - 2PS\alpha(\alpha + 1). \end{aligned} \quad (33)$$

Restoring the dimensions leads the proper a_z component of the acceleration to the form

$$a_z = \frac{c^2}{M} \ddot{z}. \quad (34)$$

IV. PROPER ACCELERATION ALONG THE ρ AXIS

In the same way as in the previous section, we compute the dimensionless proper acceleration $\ddot{\rho}$ along ρ by differentiating (17), from which we obtain

$$\ddot{\rho} = \frac{\alpha^2 \Delta \rho^2 R_2 - 2R_1}{2\alpha^2 \Delta^2 U^2 \rho^3}, \quad (35)$$

with

$$R_1 = [\alpha^4 \rho^2 P + z \Delta^2 S] \left\{ 3\alpha^4 \rho^2 P + z \Delta S + \frac{2\alpha^2 \Delta \rho^2}{U} [\alpha^2 (2\alpha^2 + 3\alpha + 1)P + a^2 z (Pz - S)] \right\}, \quad (36)$$

$$R_2 = \alpha^5 \rho^2 \{a_1 + r[2a_2 r(3a_3 + 4ra_4)]\} + 8\alpha^4 \rho^2 \{a_0 + r[a_1 + r(a_2 + r(a_3 + a_4 r))]\} + 8z\alpha^2 \Delta P S + 2\Delta^2 S(Pz - S) \\ + \frac{4\alpha^2 P}{\Delta} (\alpha^4 \rho^2 P + Sz\Delta^2) + \frac{2z\Delta^2}{S} \{2\alpha^4 P b_0 + z[2z^2 b_4 (Pz - S) + \alpha^2] b_2 (2Pz - S)\}. \quad (37)$$

Restoring the dimensions leads the proper a_ρ component of the acceleration to

$$a_\rho = \frac{c^2}{M} \ddot{\rho}. \quad (38)$$

V. t ACCELERATION

In the same way, we compute the t acceleration, i.e. the dot derivative of \dot{t} given by (19). In fact, we need

$(1/\dot{t})$, as we shall see in section VI. We obtain, by limiting ourselves to the case $L_z = 0$, which is interesting to us,

$$\left(\frac{1}{\dot{t}}\right) = \frac{2\alpha^3 T_1}{E U T_2}, \quad (39)$$

with

$$T_1 = P\alpha^3 r^2 [(a^2 - 1)^2 + 4\alpha + 2(a^2 + 3)\alpha^2 + 4\alpha^3 + \alpha^4] - 2a^2 S z r [-1 + a^4 + 2(a^2 - 1)\alpha + 2a^2 \alpha^2 + 2\alpha^3 \alpha^4] \\ - a^2 P z^2 \alpha [-3 + 2a^2 \alpha^4 + 4(a^2 - 2)\alpha + 2(a^2 - 3)\alpha^2 + \alpha^4], \quad (40)$$

$$T_2 = \{a^2 z^2 \Delta + \alpha^2 r [1 + 3a^2 + (3 + a^2)\alpha + 3\alpha^2 + \alpha^3]\}^2. \quad (41)$$

VI. OBSERVABLE VELOCITY AND ACCELERATION

We define “observable velocity and acceleration,” the set of components of the velocity and acceleration (in our case along z and ρ), as measured with the time t . These velocities and accelerations are observable at infinity, where spacetime is Minkowskian.

The time \hat{t} , the coordinate \bar{t} , which has dimensions of length like $\bar{\rho}$ and \bar{z} (see [4]), and the dimensionless coordinate t are linked by the relations

$$\hat{t} = \frac{\bar{t}}{c} = \frac{M}{c} t. \quad (42)$$

The v_z velocity is given by

$$v_z = \frac{d\bar{z}}{d\hat{t}} = \frac{M dz}{(M/c) dt} = c \frac{dz}{dt} = c \frac{\dot{z}}{\dot{t}}, \quad (43)$$

where \dot{z} and \dot{t} are given by (18) and (19), respectively. We observe that v_z is a function of ρ and z and in the limit $z \rightarrow \infty$ we have

$$\beta_z = \frac{v_z}{c} \rightarrow \left(1 - \frac{1}{E^2}\right)^{1/2}, \quad (44)$$

which is the Minkowskian expression mentioned in [6] equation (49) where we recognize that E is the Lorentz factor $\Gamma = (1 - \beta^2)^{-1/2}$ when $\beta_z \rightarrow \beta$, i.e., $\beta_\rho \rightarrow 0$. The dimensionless acceleration along z is

$$\beta'_z = \frac{d\beta_z}{dt} = \frac{1}{\dot{t}} \left(\frac{\dot{z}}{\dot{t}} \right). \quad (45)$$

Restoring the dimensions, we find that the component of acceleration along z -direction is given by

$$\gamma_z = \frac{dv_z}{d\hat{t}} = c \frac{d\beta_z}{dt} = \frac{cd\beta_z}{(M/c)dt} = \frac{c^2}{M} \beta'_z. \quad (46)$$

Similarly, the formulae for the velocity and acceleration along ρ -direction are,

$$v_\rho = c \frac{\dot{\rho}}{\dot{t}} = c \beta_\rho, \quad (47)$$

$$\beta'_\rho = \frac{d\beta_\rho}{dt} = \frac{1}{\dot{t}} \left(\frac{\dot{\rho}}{\dot{t}} \right), \quad (48)$$

where

$$\gamma_\rho = \frac{dv_\rho}{d\hat{t}} = \frac{c^2}{M} \beta'_\rho. \quad (49)$$

The conversion coefficient c^2/M from the dimensionless to the dimensional observable accelerations (46) and (49) is the same as for the proper accelerations in (34) and (38), and for the M87 galaxy black hole we find

$$\frac{c^2}{M} = \frac{9^{16}}{6 \times 10^9 \times 1.5 \times 10^3} = 10^4 \text{ ms}^{-2}, \quad (50)$$

for $M = 6 \times 10^9 M_\odot$, in accordance with recent evaluations [10].

Now we have all the quantities for the observable components of the velocity and acceleration as functions of ρ and z . Along the geodesics these two variables are no long independent, instead, ρ now is a function of z , which describes the trajectory that a particle follows for the given geodesic. The z and ρ components of the proper and observable velocities and accelerations now can be evaluated along the geodesic as functions of z only.

VII. ACCELERATION FOR HIGH ENERGY JETS

The trajectories followed by the particles running along the geodesics are obtained by eliminating the time between the equations of motion (17) and (18), i.e., they are the solutions of the differential equation,

$$\frac{d\rho}{dz} = \frac{P\alpha^4\rho^2 + S(\alpha^2 - A)^2z}{(Pz - S)(\alpha^2 - A)\alpha^2\rho}. \quad (51)$$

We consider special geodesics with trajectories given by (51). When $z \rightarrow \infty$, we find that $\rho \rightarrow \rho_1$, with the asymptotes

$$\rho_1 = \rho_e \left[1 + \frac{Q}{a^2(E^2 - 1)} \right]^{1/2}, \quad (52)$$

where $\rho_e = a/M$, highlighted in [6] equation (21), to account for a perfect collimation of jets. Such geodesics need that $L_z = 0$, as seen after equation (32) in [6]. This new parameter, ρ_1 , allows a new indirect interpretation of the Carter constant Q . Indeed, ρ_1 is a parameter characterizing the collimated jet's ejection.

We need to find the components (33) and (35), in order to obtain the observable components, (46) and (49), of the acceleration as functions of z . In principle this is possible since from (51) one can obtain ρ as a function of z , given initial conditions $\{\rho_i, z_i\}$. The same can be achieved for the observable velocities, (43) and (47), given as functions of z only. However such solutions can be determined only numerically. We can fix the parameters ρ_1 and E , specially for high E , which corresponds to the conspicuous part of the jet, as seen in [7].

As an example, let us take the following geodesic determined by $\rho_1 = 3.16354$, $E = 10^6$, $a/M = 0.877004$, and by the initial conditions inside the ergosphere, $\rho_i = 0.5648$, $z_i = -0.25$, which is the geodesic studied in section 4 of [7], i.e. asymptotically parallel to the z axis

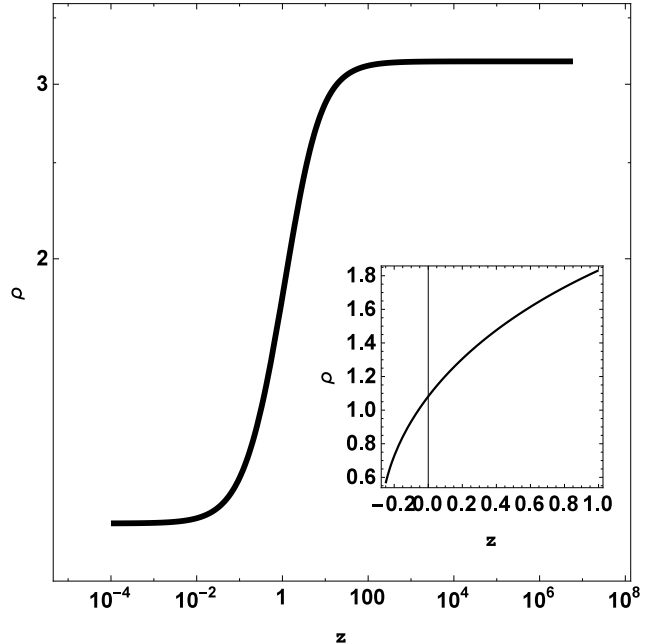


FIG. 1: LogLogPlot of the geodesic obtained by numerical integration of (51) for the parameters $a = 0.877$, $E = 10^6$, asymptotic to $\rho_1 = 3.16354$ with the initial condition $\rho_i(z_i = -0.25) = 0.5648$, for the range $z \in [10^{-4}, 6 \times 10^6]$, and (inserted inside) linear plot of the beginning for $z \in [-0.25, 1]$.

along $\rho = \rho_1$ with high energy, which is central for the M87 jet in our model (See figure 1). The trajectory of this geodesic is numerically determined by numerical integration of the differential equation (51), giving us an interpolating function $\rho = f(z)$ that we can substitute into the different precedent expressions of the velocity and acceleration, which leads us to the following results.

A. Velocity

The interpolating function $\rho(z)$ used in (43) and (47), yields a numerical solution for the observable velocity components $\beta_z(z)$ and $\beta_\rho(z)$ and norm $\beta(z)$ along this geodesic, which are plotted in figure 2. Table 1 summarizes the main numerical results. Comments on these curves and table 1 are the following.

z	\bar{z} (pc)	β_z	β_ρ	β	γ
-0.25	-0.75×10^{-4}	0.0264676	0.113153	0.116207	1.0068
0.033	10^{-5}	0.153425	0.19038	0.244441	1.0313
0.5	1.5×10^{-4}	0.284537	0.196846	0.345991	1.0658
0.75	2.25×10^{-4}	0.336773	0.188696	0.386034	1.084
2	6×10^{-4}	0.510814	0.134569	0.528242	1.1777
4.25	1.24×10^{-3}	0.670313	0.0713721	0.674102	1.3538
5	1.5×10^{-3}	0.7036	0.0591092	0.706079	1.4122
10	3×10^{-3}	0.825586	0.0220434	0.825881	1.7735
20	6×10^{-3}	0.90593	0.00668179	0.905955	2.3620
33	10^{-2}	0.942018	0.00258397	0.942021	2.9801
50	1.5×10^{-2}	0.96087	0.00118779	0.96087	3.6101
70	2.1×10^{-2}	0.971863	6.175×10^{-4}	0.971863	4.2454
100	0.03	0.980209	3.07×10^{-4}	0.980209	5.0514
333	0.1	0.994018	2.8×10^{-5}	0.994018	9.1561
500	0.15	0.996008	1.2×10^{-5}	0.996008	11.203
10^3	0.3	0.998002	3.15×10^{-6}	0.998002	15.827
10^4	3	0.9998	3.16×10^{-8}	0.9998	50.003
10^5	30	0.99998	3.1×10^{-10}	0.99998	158.11
10^6	300	0.9999980	10^{-11}	0.999998	500.0

Table 1. Some indicative values of the observable velocity (components β_z , β_ρ and norm β) and Lorentz factor (γ) as functions of z along the geodesic asymptotic to $\rho_1 = 3.1635$ for a particle of observable energy $E = 10^6$ (in units of its mass) with initial conditions $\rho_i(z_i = -0.25) = 0.5648$ inside the Kerr ergosphere of the M87 BH of mass $M = 6 \times 10^9 M_S$. See figure 2. The initial values are $\beta_{zi} = 0.026$ and $\beta_{\rho i} = 0.113153$. These initial observable velocities are non relativistic (NR).

When $z = 10^6$ for M87, taking the recent value obtained for M [10], that corresponds to $\bar{z} = 10^6 M \simeq 10^6 \times 6 \times 10^9 \times M_\odot = 6 \times 10^{15} \times \frac{3}{2} \text{ km} = 9 \times 10^{15} \text{ km} = 9 \times 3.241 \times 10^{15} \times 10^{-14} \text{ pc} = 291.69 \text{ pc} \simeq 300 \text{ pc}$, the values are $\beta_z = 0.999998$ and $\beta_\rho \approx 10^{-11}$. At the infinity, the observable Lorentz factor tends to its maximum possible value $\gamma_\infty = \sqrt{E^2 - 1} \simeq E = 10^6$ (see equations (47) and (48) in [6], and figure 5 in [11]), which is ultra-relativistic (UR). For an electron or a proton, it corresponds to the energy $\sqrt{\delta_1} \gamma \simeq 0.5 \times 10^{12} \text{ eV}$, or 10^{15} eV , respectively.

We observe that β_ρ has a (very) weakly relativistic maximum ≈ 0.2 for $z \simeq 0.5$, then rapidly becomes non relativistic and tends to zero, while the component β_z becomes relativistic, $\beta_z \sim 0.8$, near $z \sim 10$, and ultra relativistic, $\beta_z \sim 0.98$, near $z \sim 100$. The curve figure 2c shows that $\beta(z)$ becomes rapidly very close to the curve presented in figure 2a for $\beta_z(z)$.

These results (specially the shape of the curve $\beta_z(z)$ and the limit of β_z when $z \rightarrow \infty$) qualitatively remain in accordance with those obtained in [11] from different conditions ($a = 0.5$, $Q < 0$).

We remark that the shape of the curve in figure 2a (or 2c) is very similar to those obtained from recent observations (see the bottom part of figure 3 in [12]), though the assumptions (involving a magnetic field) from which they interpret the observations are very different from ours. However, their transition (from $\beta \sim 0.5$ NR to

$\beta \sim 0.9$ UR) is located to about $r \in [0.3, 1] \text{ pc}$, while ours, located about $z \in [2, 20]$, i.e., $\bar{z} \in [0.6, 6] \times 10^{-3} \text{ pc}$, is more abrupt. Besides, our model predicts that the phenomenon happens earlier (closer to the core) than that happening in their model. In fact, from figure 3 of [12], one can see that the range is from 10^{-2} to 10^2 pc , with a transition between 10^{-1} and 10 pc , while in our model, as can be seen from our figure 2c, the range runs from about 10^{-4} to 1 pc , with a transition between 10^{-4} and 10^{-2} pc . We shall come back to this issue in Section VIII.

Observations are done by the radiation emitted by the jet. It is accepted that the main source of this radiation is synchrotron radiation, which is continuous. What is observed is an almost continuous sequence of frequencies increasingly elevated to as we ascend from the stream to its source, e.g. [14–16]

Most of the methods for determining the acceleration of the jet are model-dependent: they assume that the electromagnetic field plays the dual roles: the cause of the acceleration and the creation of the synchrotron effect. But it can be also considered a situation where the cause of the accelerator is different from the origin of the synchrotron effect. This is the case of our model, where the origin of the acceleration is gravitational, while the particle accelerated to some speed will enter a magnetic field, whereby generating the synchrotron radiation. The magnetic field acts like an accelerator, but weak, and the energy gained by the particles will be quickly

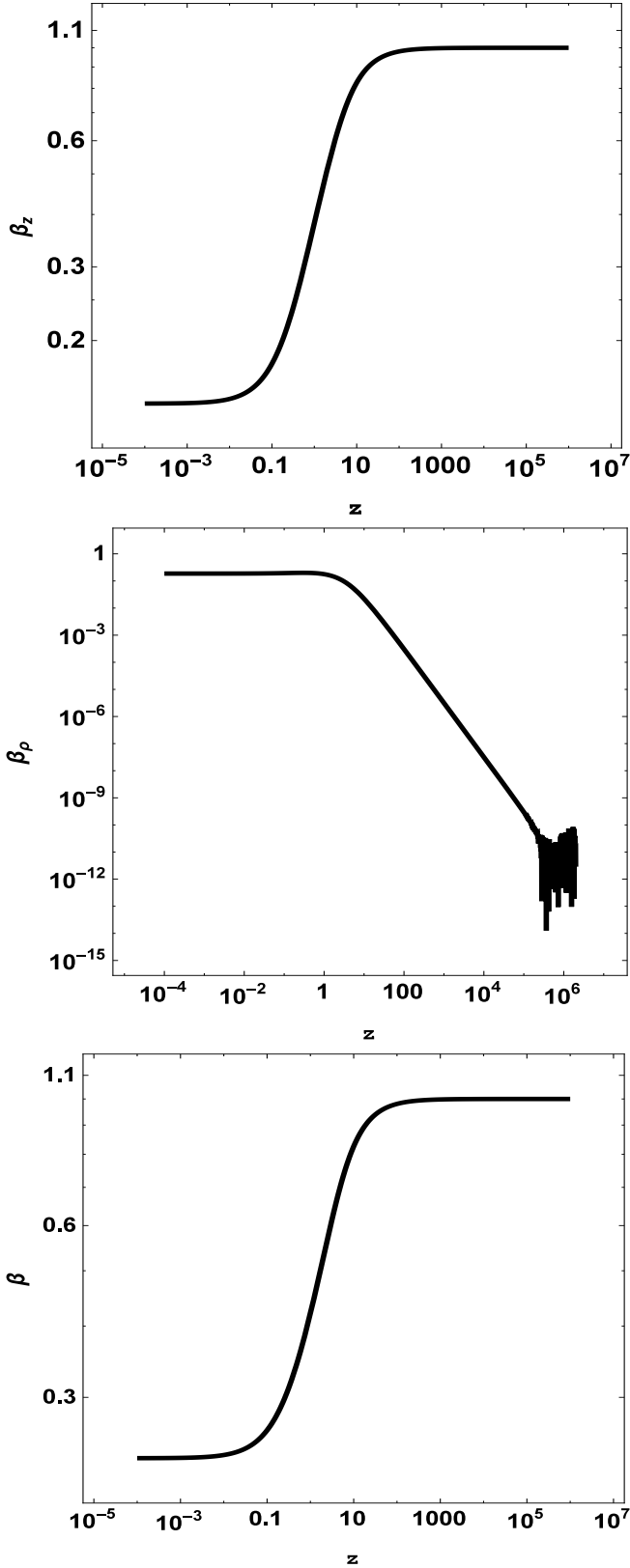


FIG. 2: Plots in LogLog scale of the observable velocity in function of z along the geodesic plotted in figure 1. Components $\beta_z = v_z/c$ (43), $\beta_\rho = v_\rho/c$ (47) and norm $\beta = (\beta_z^2 + \beta_\rho^2)^{1/2}$.

lost through radiation, making inefficient the magneto-accelerator phenomenon over long distances. The observed critical frequency is proportional to $B\gamma^2$. At the same z , the critical synchrotron frequency has a bigger Lorentz factor than that in the magnetic models, which means that the magnetic field deduced from our model is smaller than the one deduced from the previous ones.

B. Acceleration

The proper and observable accelerations are shown in figures 3, 4, 5 and 6, respectively. Table 2 summarizes the main (numerical results). Some comments on these curves and table 2 are in order.

1. Proper acceleration

Introducing the interpolating function in the proper acceleration components extracted from equations (33) and (35), yields \ddot{z} and $\ddot{\rho}$ as functions of z only along the geodesic, functions that are plotted in figures 3 and 4, respectively.

(i) Examining figure 3 in detail, we have the following remarks. The dimensionless proper acceleration \ddot{z} starts from a large positive initial value $\ddot{z}_i = \ddot{z}_{\max} = 1.5755 \times 10^{12}$ ($a_{zi} = 1.57 \times 10^{16} \text{ ms}^{-2}$), and then decreases while remaining positive (repulsive force) until $z \simeq 625$ ($\bar{z} = 625 \times M = 625 \times 6 \times 10^9 \times 1.5 \text{ km} = 5.625 \times 10^{12} \text{ km} = 0.18231 \text{ pc}$), where it vanishes. Beyond that point, it becomes negative (attractive force) until it reaches its smallest value $\ddot{z} \simeq -1.4 \times 10^{-6}$ ($a_z = -1.4 \times 10^{-2} \text{ ms}^{-2}$) at about $z \simeq 740$ ($\bar{z} = \frac{740}{625} \times 0.18231 \text{ pc} = 0.21586 \text{ pc}$), before beginning to increase and tending to zero, while always remaining negative. \ddot{z} reaches about -10^{-7} ($a_z = -10^{-3} \text{ ms}^{-2}$) for $z \simeq 3 \times 10^3$ ($\bar{z} = \frac{3000}{625} \times 0.18231 \text{ pc} = 0.87509 \text{ pc}$), and then -2×10^{-9} ($a_z = -2 \times 10^{-5} \text{ ms}^{-2}$), for $z \simeq 2.2 \times 10^4$ ($\bar{z} = \frac{2.2 \times 10^4}{625} \times 0.18231 \text{ pc} = 6.4173 \text{ pc}$). So, we can obtain the value of the (dimensionless) acceleration component \ddot{z} for each value of z all along the geodesic. In particular, $\ddot{z} \rightarrow 0$ when $z \rightarrow \infty$.

Since the initial position is the closest one to the BH, it is normal that the initial proper acceleration is maximal, meaning a maximal repulsive force, felt by the particle, in its proper (comoving) frame. The proper acceleration in a sense is the expression of the strength of the gravitational field. In Table 2 we present some particular values of these physical quantities.

(ii) On the other hand, some remarks about figure 4 are the following. Initially, we have $\ddot{\rho}_i = -8.60382 \times 10^{12}$ ($a_{\rho i} = -8.6 \times 10^{16} \text{ ms}^{-2}$). Then, it increases to $\ddot{\rho} = -7.79134 \times 10^9$ ($a_\rho = -7.79 \times 10^{13} \text{ ms}^{-2}$) at $z = 4.25$ ($\bar{z} = \frac{4.25}{625} \times 0.18231 = 1.2397 \times 10^{-3} \text{ pc}$), and abruptly becomes positive $\ddot{\rho} = +9.89455 \times 10^7$ ($a_\rho = 9.9 \times 10^{11} \text{ ms}^{-2}$) at $z = 4.95$ ($\bar{z} = \frac{4.95}{625} \times 0.18231 = 1.444 \times 10^{-3} \text{ pc}$, where a_z is slightly greater than a_ρ). It vanishes between these two last positions, for $z \simeq 4.938173812$,

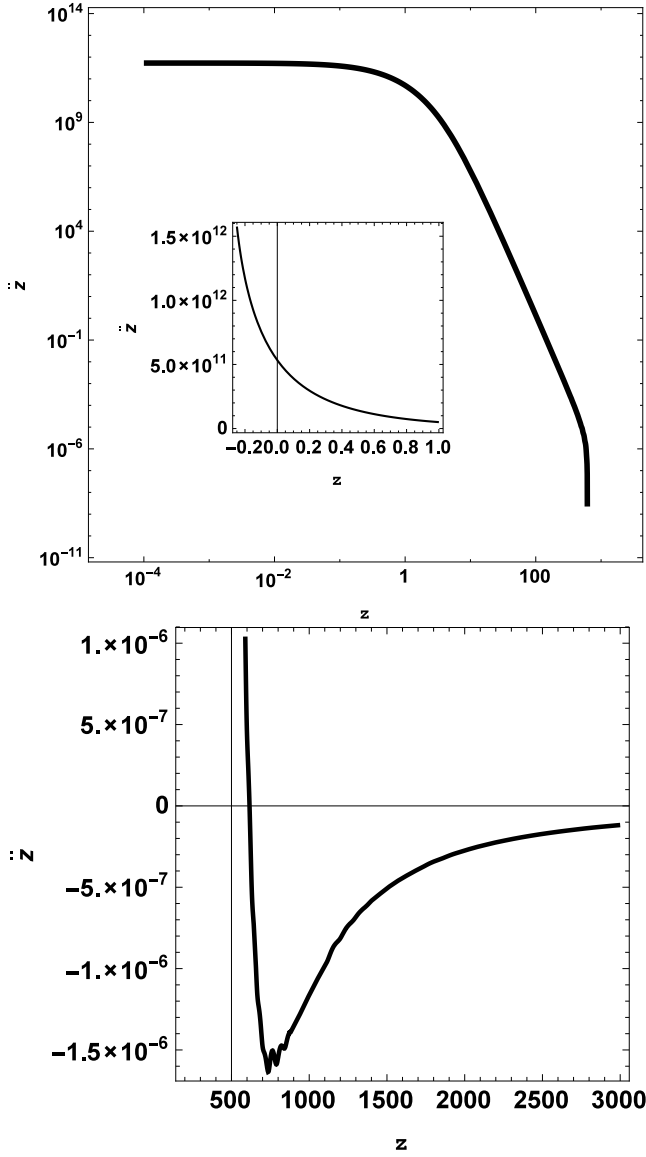


FIG. 3: Plots of \ddot{z} , the z -component of the proper acceleration (33), along the geodesic of the figure 1, in function of z . General plot in LogLog scale and two local linear plots for two different ranges : $z \in [-0.25, 1]$, starting from a maximum (inserted inside), and $z \in [10^2, 3 \times 10^3]$, showing the minimum. There is a final increasing towards zero by negative values.

from which it positively increases towards a maximum $\ddot{\rho}_{\max} = +8.71056 \times 10^9$ ($a_\rho = 8.7 \times 10^{13} \text{ ms}^{-2}$) at $z = 8.308$ ($\bar{z} = \frac{8.308}{625} \times 0.18231 \text{ pc} = 2.4234 \times 10^{-3} \text{ pc}$). Then, it decreases towards zero while remaining always positive. For the sake of comparison with \ddot{z} we note that: at $z = 30$, $\ddot{\rho} = 1.89417 \times 10^9$ (about 10^6 times greater than \ddot{z}) ; At $z = 100$, $\ddot{\rho} = 2.03259 \times 10^8$ (about 10^8 greater than \ddot{z}). At $z = 625$ (where \ddot{z} vanishes), $\ddot{\rho} = 5.48651 \times 10^6$. At $z = 740$ (where \ddot{z} is minimum and negative $\sim -10^{-6}$), $\ddot{\rho} = 3.91956 \times 10^6$; at $z = 4 \times 10^3$, $\ddot{\rho} = 1.35023 \times 10^5$. At $z = 10^4$, $\ddot{\rho} = 2.16227 \times 10^4$; at $z = 3 \times 10^5$, $\ddot{\rho} = 20$; and at $z = 10^6$, $\ddot{\rho} = 2.16$. Finally,

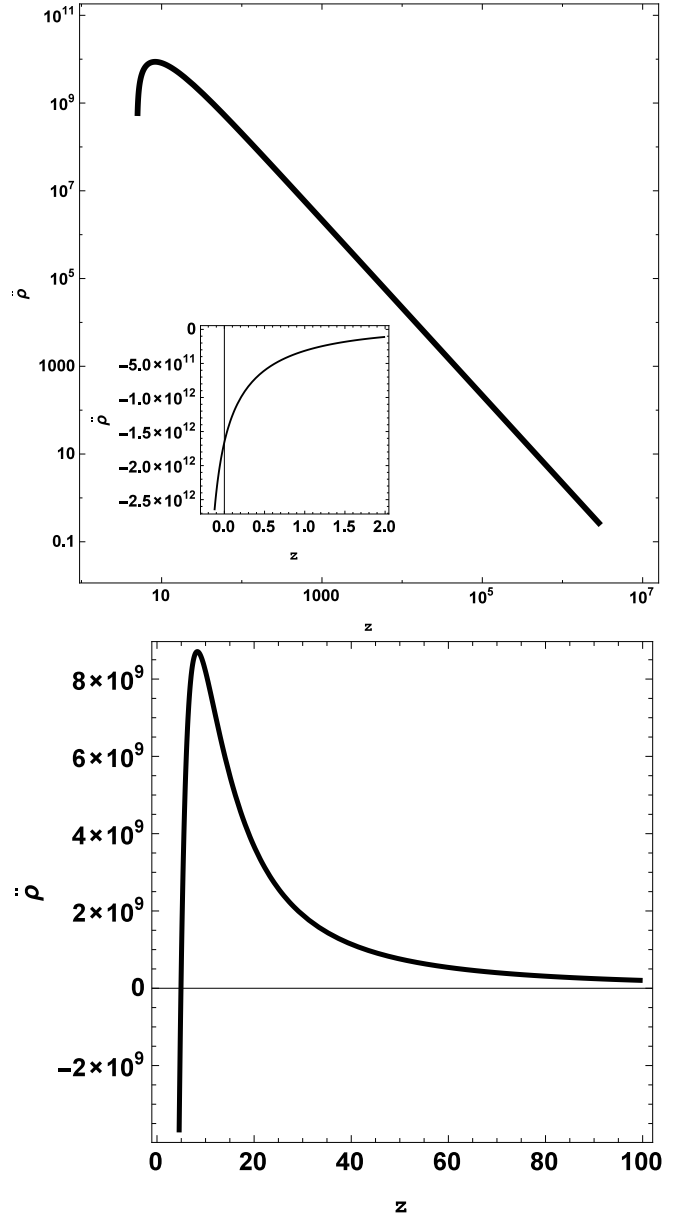


FIG. 4: Plots of $\ddot{\rho}$, the ρ -component of the proper acceleration (35), along the geodesic of the figure 1, in function of z . General plot in LogLog scale and two local linear plots for the following ranges of z : $[-0.25, 2]$ showing the beginning (inserted inside), and $[1, 10^2]$ showing the maximum. There is a final decreasing towards zero by positive values.

we have $\ddot{\rho} \rightarrow 0$, when $z \rightarrow \infty$.

2. Observed acceleration

We also plot the observed dimensionless acceleration components β'_z of (45) in figure 5 and β'_ρ of (48) in figure 6, by using the time of the observer t , instead of the proper time τ . Then, from (46) and (49) we deduce the observed dimensional accelerations γ_z and γ_ρ . In the

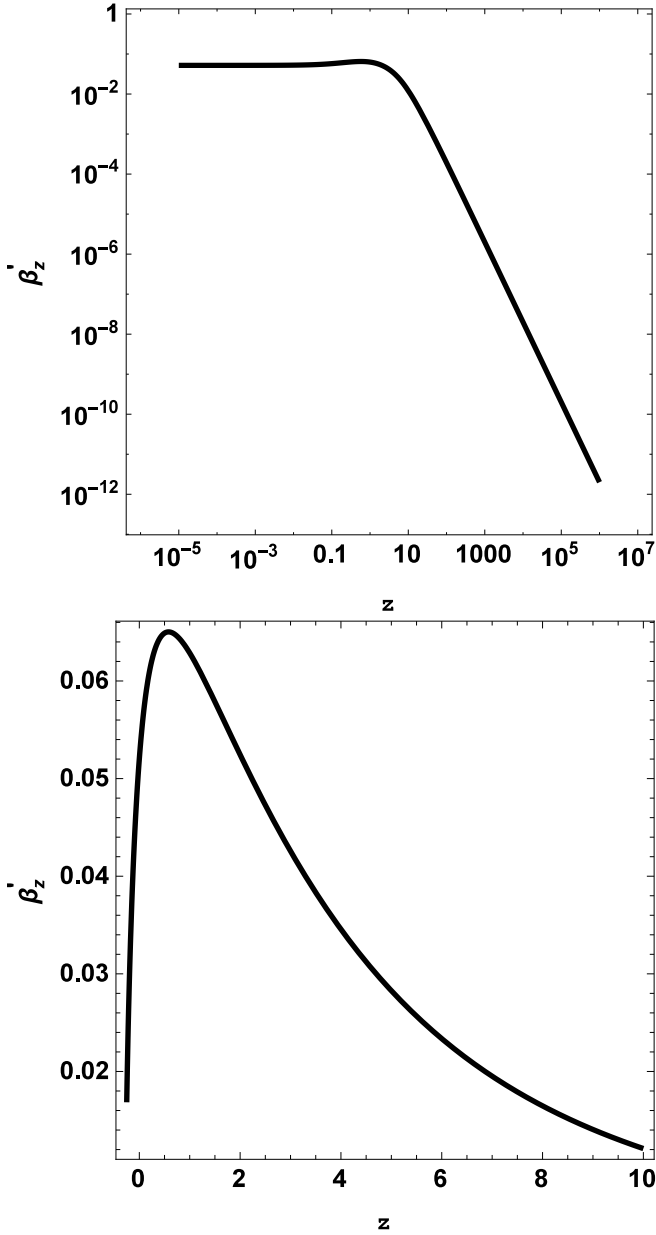


FIG. 5: Plots of the z -component β'_z of the observable acceleration (45), along the geodesic of the figure 1, in function of z . General plot in LogLog scale, and one local linear plot for the z -range $[-0.25, 10]$. Beyond, it decreases to zero. It is always positive.

following, let us consider these figures in some detail.

(i) For β'_z . We first note that it is always positive. Its initial value, at $z_i = -0.25$, is $\beta'_{zi} = 0.0168428$, i.e., $\gamma_{zi} = 168.428 \text{ ms}^{-2}$. It increases until its maximal value, $\beta'_{z\text{max}} = 0.065$ (or $\gamma_{z\text{max}} = 650 \text{ ms}^{-2}$), obtained at $z = 0.75$. Then, it decreases, by remaining always positive. At $z = 4.25$, $\beta'_z = 0.0328446$ (or $\gamma_z = 328.4 \text{ ms}^{-2}$), at $z = 10$, $\beta'_z = 0.012103$ (or $\gamma_z = 121 \text{ ms}^{-2}$), at $z = 30$, $\beta'_z = 0.00191447$ (or $\gamma_z = 19.15 \text{ ms}^{-2}$), at $z = 100$, $\beta'_z = 0.000191857$ (or $\gamma_z = 1.92 \text{ ms}^{-2}$), at

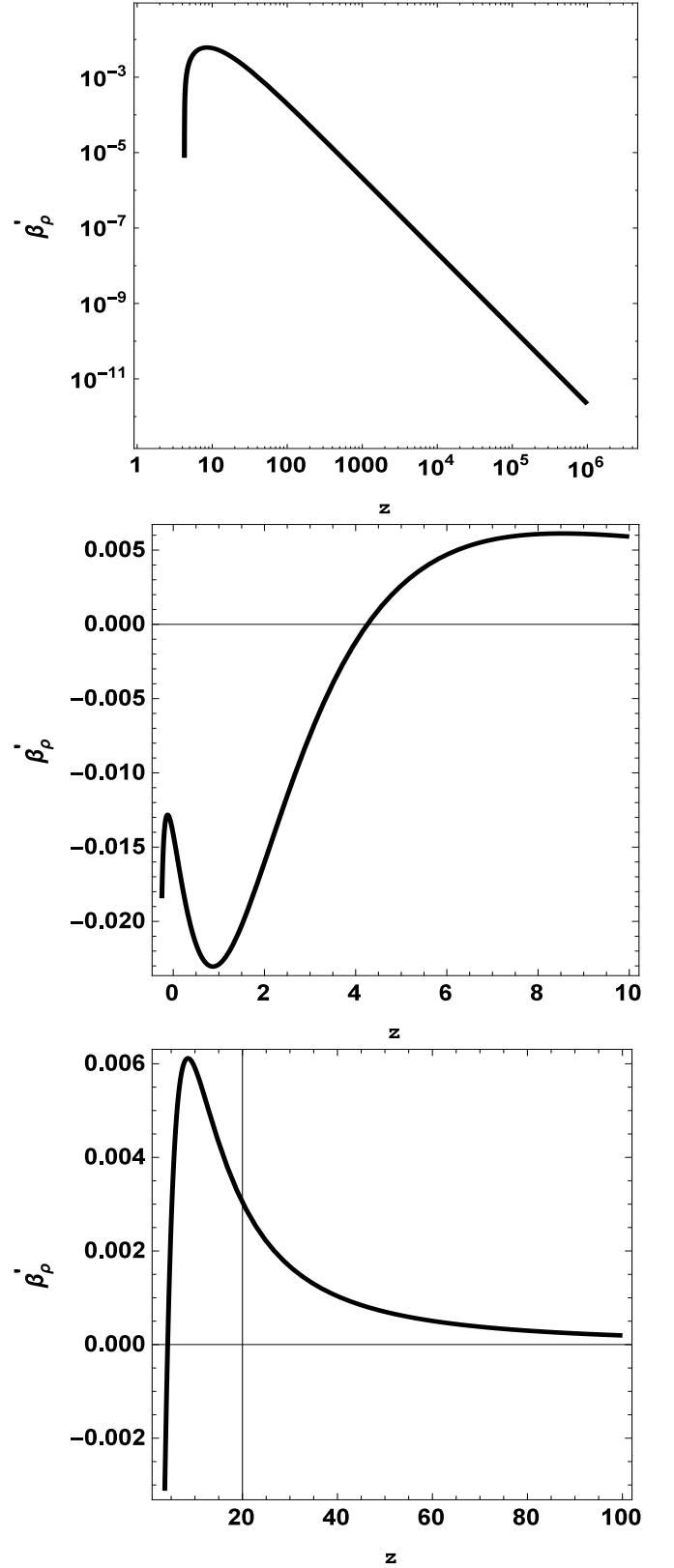


FIG. 6: Plots of the ρ -component β'_ρ of the observable acceleration (48), along the geodesic of the figure 1, in function of z . General plot in LogLog scale, and two local linear plots for the z -ranges $[-0.25, 10]$, showing the oscillation at the beginning, and $[3, 10^2]$ showing the maximum. There is a final decreasing to zero. It is always positive beyond $z \sim 4.5$.

$z = 200$, $\beta'_z = 4.89903 \times 10^{-5}$ (or $\gamma_z = 5 \times 10^{-1} \text{ ms}^{-2}$), at $z = 625$, $\beta'_z = 5.08713 \times 10^{-6}$ (or $\gamma_z = 5.1 \times 10^{-2} \text{ ms}^{-2}$), at $z = 740$, $\beta'_z = 3.6325 \times 10^{-6}$ (or $\gamma_z = 3.6 \times 10^{-2} \text{ ms}^{-2}$), at $z = 4 \times 10^3$, $\beta'_z = 1.24875 \times 10^{-7}$ (or $\gamma_z = 1.25 \times 10^{-3} \text{ ms}^{-2}$), at $z = 10^4$, $\beta'_z = 1.992 \times 10^{-8}$ (or $\gamma_z = 2 \times 10^{-4} \text{ ms}^{-2}$), at $z = 3 \times 10^5$, $\beta'_z = 2.22219 \times 10^{-11}$ (or $\gamma_z = 2.2 \times 10^{-7} \text{ ms}^{-2}$), and at $z = 10^6$, $\beta'_z = 1.999 \times 10^{-12}$ (or $\gamma_z = 2 \times 10^{-8} \text{ ms}^{-2}$). Finally, we find that $\beta'_z \rightarrow 0$, when $z \rightarrow \infty$.

(ii) For β'_ρ . We see that it begins with negative values at $z_i = -0.25$, $\beta'_{\rho i} = -0.0184435$ (or $\gamma_{\rho i} = -184.4 \text{ ms}^{-2}$), then increases until its first (secondary) maximum, always negative, $\beta'_\rho = -0.0128256$ (or $\gamma_\rho = -128.2 \text{ ms}^{-2}$) at $z = -0.1255$, then decreases until its minimum $\beta'_\rho = -0.02304375$ (or $\gamma_\rho = -230.44 \text{ ms}^{-2}$) reached at $z = 0.870$. Then it increases again, at $z = 2$, $\beta'_\rho = -0.0160365$ (or $\gamma_\rho = -160.4 \text{ ms}^{-2}$), at $z = 4.2579615$, $\beta'_\rho = 0$ (or $\gamma_\rho = 0 \text{ ms}^{-2}$). Then it becomes positive, always increasing, until its (main) max-

imum $\beta'_\rho = +0.00611618$ (or $\gamma_\rho = 61.2 \text{ ms}^{-2}$) reached at $z = 8.5275$, from which it decreases again, remaining positive, towards zero. At $z = 10$, $\beta'_\rho = 0.00590862$ (or $\gamma_\rho = 59.1 \text{ ms}^{-2}$), at $z = 30$, $\beta'_\rho = 0.00166611$ (or $\gamma_\rho = 16.7 \text{ ms}^{-2}$), at $z = 100$, $\beta'_\rho = 1.95353 \times 10^{-4}$ (or $\gamma_\rho = 2 \text{ ms}^{-2}$), at $z = 200$, $\beta'_\rho = 5.14424 \times 10^{-5}$ (or $\gamma_\rho = 0.5 \text{ ms}^{-2}$), at $z = 625$, $\beta'_\rho = 5.45155 \times 10^{-6}$ (or $\gamma_\rho = 5.4 \times 10^{-2} \text{ ms}^{-2}$), at $z = 740$, $\beta'_\rho = 3.89845 \times 10^{-6}$ (or $\gamma_\rho = 3.4 \times 10^{-2} \text{ ms}^{-2}$), at $z = 4 \times 10^3$, $\beta'_\rho = 1.34888 \times 10^{-7}$ (or $\gamma_\rho = 1.35 \times 10^{-3} \text{ ms}^{-2}$), at $z = 10^4$, $\beta'_\rho = 2.16141 \times 10^{-8}$ (or $\gamma_\rho = 2.16 \times 10^{-4} \text{ ms}^{-2}$), at $z = 3 \times 10^5$, $\beta'_\rho = 2.40387 \times 10^{-11}$ (or $\gamma_\rho = 2.4 \times 10^{-7} \text{ ms}^{-2}$), at $z = 10^6$, $\beta'_\rho = 2.16365 \times 10^{-12}$ (or $\gamma_\rho = 2.16 \times 10^{-8} \text{ ms}^{-2}$), and finally $\beta'_\rho \rightarrow 0$ (or $\gamma_\rho = 0 \text{ ms}^{-2}$) when $z \rightarrow \infty$.

The two components of the acceleration are positive from $z = 4.25$ until the infinity, with fairly large positive values until $z \simeq 20$ to 30 (at $z = 10$, $\beta'_z = 0.012$, $\beta'_\rho = 0.006$).

z	z (pc)	\ddot{z}	$\ddot{\rho}$	β'_z	β'_ρ
-0.25	-0.75×10^{-4}	1.57549×10^{12}	-8.60382×10^{12}	1.68428×10^{-2}	-1.84435×10^{-2}
0.75	2.25×10^{-4}		-4.26388×10^{11}	6.5×10^{-2}	-2.29007×10^{-2}
0.9	2.7×10^{-4}			6.36627×10^{-2}	-2.30357×10^{-2}
2	6×10^{-4}	9×10^9	-1.103×10^{11}		-1.60365×10^{-2}
4.25	1.2397×10^{-3}		-7.79134×10^9	3.28446×10^{-2}	0
4.95	1.444×10^{-3}	2.71515×10^8	9.89455×10^7	2.85532×10^{-2}	2.47246×10^{-3}
10	3×10^{-3}	5.98106×10^6	8.19×10^9	1.2103×10^{-2}	5.90862×10^{-3}
30	9×10^{-3}	5272.53	1.89417×10^9	1.91447×10^{-3}	1.66611×10^{-3}
10^2	0.03	1.39406	2.03259×10^8	1.91857×10^{-4}	1.95353×10^{-4}
200	0.06	10^{-2}	5.24775×10^7	4.89903×10^{-5}	5.14424×10^{-5}
500	0.15	10^{-5}	8.552115×10^6	7.93574×10^{-6}	8.4861×10^{-6}
625	0.18231	0	5.48651×10^6	5.08713×10^{-6}	5.45155×10^{-6}
740	0.222	-1.4×10^{-6}	3.91956×10^6	3.6325×10^{-6}	3.89845×10^{-6}
10^3	0.3	-1.1×10^{-6}	8.15083×10^6	1.99198×10^{-6}	2.14225×10^{-6}
4×10^3	1.2	-0.6×10^{-7}	1.35023×10^5	1.24875×10^{-7}	1.34888×10^{-7}
10^4	3	-0.2×10^{-7}	2.16227×10^4	1.992×10^{-8}	2.16141×10^{-8}
3×10^5	90	-10^{-11}	20	2.22219×10^{-11}	2.40387×10^{-11}
10^6	300	-1.00002×10^{-12}	2.16366	1.999×10^{-12}	2.16365×10^{-12}

Table 2. Some indicative values of proper and observable acceleration components along the same geodesic than in table 1. See the corresponding plots figures 3 to 6.

VIII. DISCUSSION AND CONCLUSION

In review of what were presented in the above sections, we find the following: at the initial, the observable velocities are NR (very weakly relativistic), and the energy is dominated by the potential, as can be seen from the high initial values of the proper acceleration. At the end, when $z \rightarrow \infty$, $\ddot{z} \rightarrow 0$ and $\ddot{\rho} \rightarrow 0$ (particles are free of gravitation) and $\beta_z \rightarrow \beta \equiv [(\gamma^2 - 1)/\gamma^2]^{1/2}$, $\beta_\rho \rightarrow 0$ (UR particles), i.e., at the infinity, energy became fully kinetic ($E = \gamma$, where γ is the Lorentz factor.). The observable,

z -acceleration, is positive all along the geodesic until the infinity. The z -acceleration reaches a maximum and then decreases until zero. The observable ρ -acceleration is negative (attractive force) from the initial until $z \approx 4.26$, at which it vanishes, and then becomes positive (repulsive force) until it reaches its maximum value at $z \simeq 8.5275$ before to tend to zero again. There is a permanent repulsive force along the two axes from $z \gtrsim 4.5$ until $z \simeq 20$, and then tending to zero at the infinity.

The transition from NR ($\beta \approx 0.5$) to UR ($\beta \approx 0.97$) is in a sub-parsec scale, in accordance with the recent ob-

servations [12], though our model predicts a more abrupt transition closer to the core. This discrepancy can be understood as follows. The results of [12] are the averages over more than 100 cases, and it could be possible that the case of a more powerful jet is different from these averaged ones. However, for M87 there is no improvement (See section 4.3 of [25]) by suggesting a jet acceleration from $0.01c$ to $0.97c$ on the z -range $[4 \times 10^2, 10^6]$. There were only two exceptions, observed at $43GHz$ with VLBA [26, 27], indicating possible ultra-relativistic bulk speeds of the M87 jet from 4×10^{-2} pc, which is in favor of our results. An interesting discussion on this point is made by Asada et al. given in section 4.3 of [25]. Very recently, Mertens et al. [28] highlighted a triple filamentary structure of the jet at the scales $z \in [10^2, 10^3]$ with a fast interior stream with $\beta \sim 0.92$. But, in more general cases, upstream (nearer the origin) results are missing. Lee et al. noted in their discussions (see section 4 of [12]) that there are only 3 data in the range 10^{-2} to 10^{-1} pc. Further observations will permit to see if the hypothesis of a spine component, narrower around the axis and more energetic, is verified.

We first note that with the high value 10^6 for E we could explain the early acceleration. However, we also made the same evaluations of the Lorentz factor γ for various values ($20, 10^2, 10^3$ and 10^9) of the energy E . The results, which we did not reproduce here, actually remain the same, and in particular the transition zones (from NR to UR) and the slopes do not change dramatically. A general explanation of this discrepancy could be that our calculations are made in vacuum, while one expects that the jet is inside a magnetized medium, which produces a braking effect. The main theoretical difficulty is that there is no known exact Kerr solution inside a medium, so all proposed solutions, including the magnetic models, remain approximated. However, we cannot ignore the gravitational effect highlighted here which seems to be the main one, in the sense that it happens earlier and more abruptly than the magnetic effect which can transform the internal energy, including the magnetic energy, into kinetic energy.

In support of the above explanation, we note that the position r of the origin of the synchrotron emission at a given frequency is evaluated from the synchrotron power (equation (7) in [12]), which depends on the product $(B\gamma)^2$. Thus, for each given altitude z , the same measure

of the power L_S can correspond to different values of γ and B , for example a large value of γ and a small value of B , as long as the product $B\gamma$ remains the same. In particular, this implies that in our model the magnetic field can be smaller than that in their models. This is consistent with our model in which the magnetic field is disruptive as least as possible, so that the main effect will be gravitational.

The remarkable straightness of the observed jet all along its length ($\approx 10^3$ kpc) is ensured by the existence of a positive acceleration at the very early time (from $z \approx 4.5$) on a very large scale (theoretically until infinity). Though progressively decreasing, the repulsive acceleration is present all the way to infinity. Besides, the bremsstrahlung radiation (in its own electromagnetic field) is negligible in our model. In fact we expect that the gravito-magnetic field [13, 17–24] plays the role of a magnetic field for the acceleration and collimation of the jet.

As the Blandford-Payne [2] mechanism can complement the Blandford-Znajek effect [1] in the magnetic paradigm for the jet formation, the Poirier-Matthews mechanism [24] can complement our BH effect [6] in the gravitomagnetic paradigm. This explanation of the formation of extragalactic jets can be tested in the future by probing the gravitomagnetic structure inherent to Einstein's general relativity.

In addition, the electromagnetic field plays no role for neutral particles, while a gravitational model, similar to ours, can explain the presence of neutral particles in the formation of jets. In particular, this gravitational model can be useful to model the ejection of VHE particles [29], including neutral particles such as neutrinos.

Acknowledgements

Part of the work was carried out when A.W. was visiting the State University of Rio de Janeiro (UERJ), Brazil. A.W. would like to express his gratitude to UERJ for hospitality. This work is supported in part by Ciência Sem Fronteiras, No. 004/2013 - DRI/CAPES, Brazil (A.W.); Chinese NSF Grant Nos. 11375153 (A.W.) and 11675145 (A.W.).

-
- [1] R. D. Blandford and R. L. Znajek *Mon. Not. R. Astron. Soc.* **179** 433 (1977).
 - [2] R. D. Blandford and D. G. Payne *Mon. Not. R. Astron. Soc.* **199** 883 (1982).
 - [3] B. Punsly *Black Hole Gravitohydromagnetics* 2nd edition, (Berlin: Springer Verlag) (2008).
 - [4] S. Chandrasekhar *The Mathematical Theory of Black Holes* (Oxford: Oxford University Press) (1983).
 - [5] J. Bičák, O. Semerák and P. Hadrava, *Month. Not. R.*

- Astron. Soc.* **263** 545 (1993).
- [6] J. Gariel, M. A. H. MacCallum, G. Marçilhac and N. O. Santos *Astron. and Astrophys.* **515** A15 (2010).
- [7] J. Gariel, G. Marçilhac and N.O. Santos *Astrophys. J.* **774** 109 (2013).
- [8] J. Gariel, N. O. Santos and J. Silk *Phys. Rev. D* **90** 063505 (2014).
- [9] J. Gariel, N. O. Santos and A. Wang *Gen. Rel. Grav.* **48** 66 (2016).

- [10] K. Gebhardt, J. Adams, D. Richstone, T. R. Lauer, S. M. Faber, K. Gültekin, J. Murphy and S. Tremaine *Astrophys. J.* **729** 119 (2011).
- [11] J. A. de Freitas Pacheco, J. Gariel, G. Marclhacy and N. O. Santos *Astrophys. J.* **759** 125 (2012).
- [12] S. S. Lee, A. P. Lobanov, T. P. Krichbaum and J. A. Zensus *arXiv:1604.02207v1 [astro-ph.GA]* (2016).
- [13] D. Tsoubelis, A. Economou and E. Stoghianidis *Phys. Rev. D* **36** 1045 (1987).
- [14] K. Asada and M. Nakamura *Astrophys. J.* **745** L28 (2012).
- [15] K. Hada et al. *Nature* **477** 185 (2011).
- [16] K. Hada et al. *Astrophys. J.* **775** 70 (2013).
- [17] W. B. Bonnor *Class. Quantum Grav.* **12** 499 (1995).
- [18] W. B. Bonnor and B. R. Steadman *Class. Quantum Grav.* **16** 1853 (1999).
- [19] L. Herrera and N. O. Santos *J. Math. Phys.* **42** 4956 (2001).
- [20] D. Bini, C. Cherubini, R. T. Jantzen and B. Mashhoon *Class. Quantum Grav.* **20** 457 (2003).
- [21] G. V. Kraniotis *Class. Quantum Grav.* **24** 1775 (2007).
- [22] C. Chicone and B. Mashhoon *Phys. Rev. D* **83** 064013 (2011).
- [23] C. Chicone and B. Mashhoon *Phys. Lett. A* **375** 957 (2011).
- [24] J. Poirier and G. J. Mathews *Class. Quantum Grav.* **33** 107001 (2016).
- [25] K. Asada, M. Nakamura, A. Doi, H. Nagai and M. Inoue *Astrophys. J.* **781** L2 (2014).
- [26] V. A. Acciari et al. *Science* **352** 444 [2009].
- [27] R. C. Walker, C. Ly, W. Junor and P. E. Hardee *JPhCS* **131** 012053 (2008).
- [28] F. Mertens, A. P. Lobanov, R. C. Walker and P. E. Hardee *arXiv:1609.0506v1 [astro-ph.HE]* (2016).
- [29] A. Abramovski et al. *Astrophys. J.* **746** 151 (2012).